Flow actuation using radio frequency in partially ionized collisional plasmas

Subrata Roy[a)]
Computational Plasma Dynamics Laboratory, Mechanical Engineering, Kettering University, Flint, Michigan 48504

(Received 15 November 2004; accepted 31 January 2005; published online 3 March 2005)

We present a multidimensional theoretical model for a better understanding and the design of the dielectric barrier discharge-induced momentum exchange. Specifically, the formulation is used to predict surface discharge using two-dimensional asymmetric electrode configurations. Model predictions for charge densities, the electric field, and gas velocity distributions are shown to mimic trends reported in the experimental literature. We also predict the electron charge accumulation on the dielectric surface self-limiting the discharge. © *2005 American Institute of Physics*. [DOI: 10.1063/1.1879097]

Recent experimental focus on radio-frequency (rf)-based dielectric surface discharge at atmospheric pressures shows tremendous potential for boundary layer flow actuation which will be useful for aerospace and many other applications.[1,2] These actuators can apply large electrohydrodynamic (EHD) forces in a relatively precise and self-limiting manner, have rapid switch-on/off capabilities and require no moving parts. Typical electrode arrangements for these devices are similar to that shown in Fig. 1 where the grounded electrode is surrounded by an insulator and a voltage fluctuating with rf is applied to the electrode exposed to the gas. The electric forces are generated through electrodes embedded in the dielectric. As the applied voltage becomes sufficiently large for a given interelectrode distance d and pressure p, the dielectric surface adjacent to the rf electrode produces a barrier discharge weakly ionizing the surrounding gas. The experimental data suggest 1–20 kV peak-to-peak applied voltage with 2–50 kHz rf is suitable for these actuators operating at atmospheric pressure. The plasma at this pressure is highly collisional causing an efficient energy exchange between charged and neutral species. In this discharge, microfilaments of nanosecond duration with many current pulses in a half-cycle maintain the optical glow.

Due to a combination of electrodynamic and collisional processes, the proper mechanism of which is yet to be theoretically resolved, charge separated particles induce the gas particles to move. For accuracy and fidelity, it is essential that the force model be derived from first principles through a simulation of the elementary mechanisms that yield the discharge. Roy and Gaitonde[3] demonstrated such a model for volume discharge between two dielectric coated electrodes using a finite element (FE)-based one-dimensional multifluid formulation for atmospheric conditions. The model was relatively basic but formed the framework of a first-principles-based methodology. Simulations showed reasonable comparison with reported rf discharges in partially ionized helium gas between two insulated electrodes.

Here, the multidimensional model for surface dielectric barrier discharge (DBD) at atmospheric pressures is presented as a first approximation. The formulation is consistent and calculates charge and neutral number densities, their momentum dynamics, electric field, and potential distribution in two spatial dimensions. For simplicity, inert helium is used as a carrier gas. The charge particle $\alpha=e,i$ distributions n_α are considered non-Maxwellian obeying the continuity relation $\partial n_\alpha/\partial t+\partial n_\alpha V_{\alpha j}/\partial x_j=n_e z-r n_e n_i$. The electron temperature is nearly uniform at 1 eV=11 600 K and the ions and neutrals are in LTE at 300 K. The working gas helium is maintained at bulk pressure $p=300$ Torr and temperature $T=300$ K. The charge momentum follows the diffusion form (neglecting inertia), $n_\alpha V_{\alpha j}=\mathrm{sgn}(e)n_\alpha\mu_\alpha E_j-D_\alpha\partial n_\alpha/\partial x_j$, where $E_j=-\partial\phi/\partial x_j$ is the electric field, and $V_{\alpha j}$ is the jth velocity component for the particle α. The potential distribution ϕ is calculated based on Poission equation, $\varepsilon(\partial^2\phi/\partial x_j^2)=-q$, where charge $q=e(n_i-n_e)$. The electron diffusion is based on the Einstein relation, $D_e=(T_e/e)\mu_e$, where T_e is the energy in electron volts, e is the elementary charge, ε is the permittivity, and $\mu_e=e/(m_e\nu_{en})$ is the mobility of an electron, where $\nu_{en}\approx 10^{12}$/s is the electron-neutral collision frequency[4] while $\nu_{in}\approx 10^9$/s. The ion diffusion $D_i=500$ cm^2/s at 300 K, and the ion mobility μ_i is given as Ref. 5. The ionization rate z for helium gas used here is $z^i/n_n=\langle V_e\sigma^i(V_e)\rangle$, the averaging is done over the velocities of the electrons whose energy is sufficient for ionization $mV_e^2/2>H_i$, the first ionization potential. The ionization process can be described as $e+\mathrm{He}\rightarrow\mathrm{He}^+ +e+e'$, where e and e' have different energy levels. The coefficient of recombination is given as $r=\langle V_{\mathrm{eth}}\sigma_{ei}^r(V_{\mathrm{eth}})\rangle=1.09\times 10^{-14}T^{-9/2}n_e$ cm^3/s. Here, V_{eth} is the electron thermal velocity and σ_{ei} is the

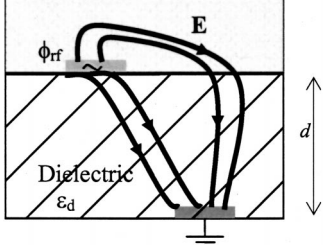

FIG. 1. Schematic of the 2D simulation domain between rf-induced dielectric barrier discharge.

[a)]Electronic mail: sroy@kettering.edu

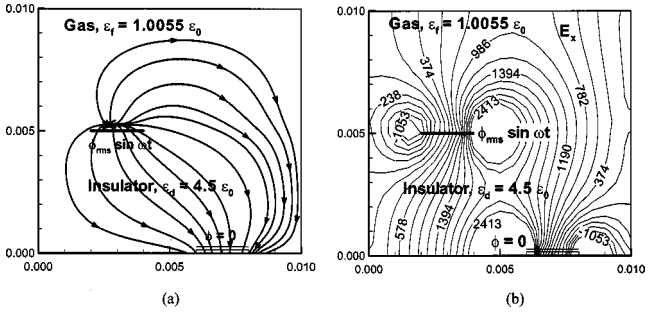

FIG. 2. Instantaneous solution for asymmetric configuration: (a) Electric-field lines, and (b) streamwise component of the electric field.

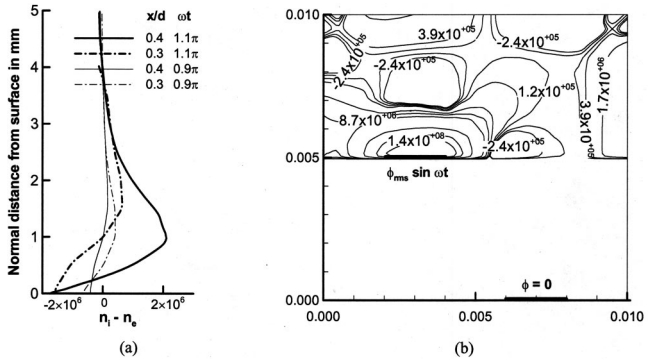

FIG. 3. Contours and line plots show negative charge accumulation on the downstream dielectric surface of the rf electrode: (a) Line plots of charge distribution at various time and spatial locations, and (b) 2D contours of $(n_i\text{-}n_e)$ at peak voltage.

electron-ion collision cross section. For simplicity, we ignored recombination effect on momentum at this stage.

Here, the electron plasma frequency, $\omega_{pe}=2e\sqrt{(\pi n_e/m_e)}$, is much higher than the applied voltage frequency. Also, the momentum exchange terms due to electron-electron and ion-ion interaction are negligible in comparison with the electron-ion and ion-neutral momentum exchange as the relative drift between similar particles is small in comparison with the drift between electrons, ions, and neutrals.

It is important to calculate the neutral dynamics consistently so as to capture the momentum transfer process accurately. The conservation of neutral particles n_n of the carrier gas at atmospheric condition follows: $\partial n_n/\partial t+\partial n_n V_{nj}/\partial x_j = -n_e z+rn_e n_i$. The dynamics of neutral particles are determined using the electron-neutral and ion-neutral collisional momentum exchange and ionization.

The averaged velocity V_f of the fluid of density ρ following $\partial\rho/\partial t+\partial\rho V_{fj}/\partial x_j=0$ is based on the Navier–Stokes equations with EHD body force: $\partial V_{fj}/\partial t+V_{fl}(\partial V_{fj}/\partial x_l) = \varpi qE_j/\rho-(RT/\rho)(\partial\rho/\partial x_j)+(\partial/\partial x_l)\tau_{jl}$, where R is the gas constant, $\tau_{jl}=\nu(\partial V_{fl}/\partial x_j+\partial V_{fj}/\partial x_l)-2/3\nu(\partial V_{fk}/\partial x_k)\delta_{jl}$ is the fluid shear tensor with ν as the gas viscosity and δ_{jl} is the Kronecker delta. The factor ϖ is introduced to modulate the effect of electric field.

The multiscale ionized gas (MIG) flow code was used to solve the charge and gas hydrodynamic equations. MIG implements a powerful high-fidelity FE procedure adapted from fluid dynamics to overcome the stiffness of the equations generated by multispecies charge separation phenomena.[6,7] FE techniques are especially suitable for their adaptability to arbitrary multidimensional geometries and boundary conditions.[8,9] Here, a two-dimensional (2D) bilinear FE formulation is employed along with implicit time marching to solve the continuity and momentum equations for all species and gas. The solution process consists of two steps—first solve for all species (including neutrals) to calculate the charge separation and electric field up to a periodic asymptote with a time step of up to 100 times the dielectric relaxation time scale,[10] then use those as body force to predict the fluid velocity and continuity evolving in time with the flow time scale. The Galerkin weak statement associated with a variational integral underlines the development of this numerical algorithm. The solution of the Newton iteration for the resulting matrices is convergent at any given time step when the maximum value of the residual relative L_2 norm for each of the state variable becomes smaller than a convergence criterion of 10^{-4}.

The computational domain $(x,y:0,0.01\text{ m})$ consists of a lower half $(y:0,0.005\text{ m})$ insulated with dielectric constant ε_d, and an upper half filled with inert helium gas of $\varepsilon_f=1.0055\ \varepsilon_0$, where ε_0 is permittivity of a vacuum. Inside the insulator, the real current is forced to zero while the displacement current is balanced with the total current at the gas-dielectric boundary. The schematic in Fig. 1 shows two electrodes in which the bottom electrode is grounded and a rf alternating frequency of 6 kHz with peak-to-peak potential of 1.6 kV is imposed at the top electrode. Each electrode is thin and 2 mm long. They are offset horizontally by 2 mm. This will be noted as asymmetric configuration. All other boundary conditions are maintained at zero flux, i.e., homogeneous Neumann boundary condition is applied.

Figure 2(a) plots the instantaneous axial electric-field distribution for an exposed anode and a grounded cathode in asymmetric configuration in the positive half of the cycle. The electric-field lines clearly represent a directional bias toward the right. The most ions accelerate toward the right along these lines leaving only a few to move in the opposite direction. The net result is an order of magnitude higher gas velocity downstream of the right edge of the exposed anode with a two orders of magnitude smaller negative velocity near the left edge. These results stress that the asymmetry enhances the electric field and thus influences flow direction. Figure 2(b) shows the development of a near circular growth of positive peak of approximately 2400 V/cm and negative trough of 1050 V/cm at the right and left end of the exposed electrode, respectively. The computed solutions are very similar to the experimental data[1,2] where the exposed electrode is situated upstream of the peak location of the electric field and thus the peak of velocity. Note that the highest value of the electric field about the edges of the grounded electrode is at least twice as much of that near the exposed electrode. The peak of the crosswise component E_y (not shown here due to space limitation) is however, just above the electrodes.

Figure 3 shows very close resemblance of the physical understanding of the DBD for the charge deposition at the surface of the dielectric.[2,11] The crosswise distributions of charge at different values of time ωt and location x/d measured from the downstream of the exposed electrode in Fig. 3(a) show how electrons accumulate over time on the dielectric surface. In surface discharge within a very short time after breakdown, the charge buildup at the dielectric surface sets off microdischarges of nanosecond duration, limiting the electric field at the location of the microdischarge such that the charge current at this position is cutoff. This has an im-

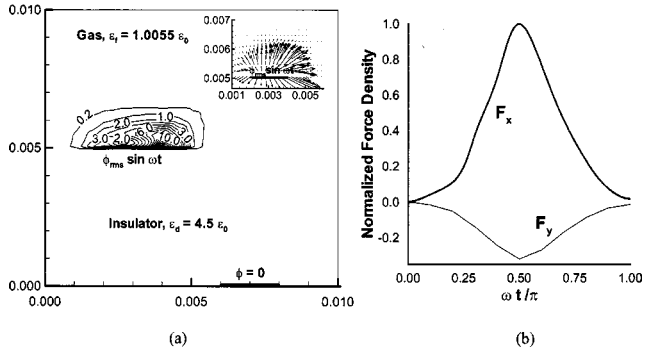

FIG. 4. (a) Charge and force details at $\pi/2$ radians shows concentrated field near the exposed electrode and (b) normalized force density distribution in the positive-half of the rf cycle.

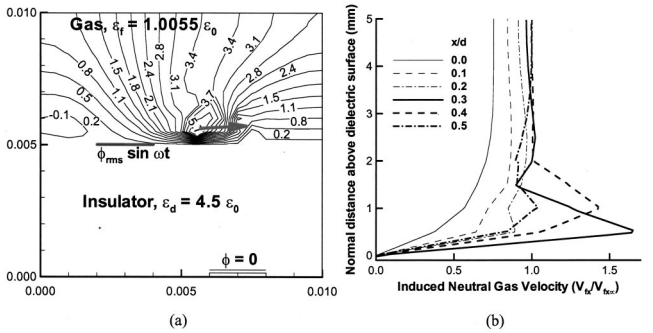

FIG. 5. (a) Streamwise component of fluid velocity computed from the force density qE_j show location of highest momentum transfer, and (b) calculated streamwise component of the gas velocity distribution at different locations along the flow.

portant effect on flow control. The small time scale of the discharge allows minimal charge transport and energy dissipation, thus less gas heating.

The 2D charge solutions plotted in Fig. 3(b) show the nonuniform nature of the distribution along the edge of the dielectric. A residual of electrons remains deposited on the dielectric surface downstream of the exposed powered electrode for the entire duration of the cycle and causes a net electric force in the direction from the electrode to the downstream surface. This is why the net near wall jet velocity is unidirectional. The peak streamwise electron current for this solution is predicted at the two corners of the exposed electrode with a maximum magnitude ($\sim$3 mA) around π radian and the minimum current ($\sim$0.2 mA) is computed for the $\pi/2$ radian. This periodic behavior of the electron current explains the charge build up on the insulator surface opposing the applied voltage just beyond the peak as the applied voltage starts decreasing, thus bounding the discharge. This is also confirmed by the experimental data (see, for example, Fig. 2 of Ref. 12) where the current magnitude peaks at about π radian.

Figure 4(a) plots the computed force due to charge separation and the electric field and shows a local maximum about the exposed electrode with nearly ten times force near the right edge as compared to the left edge. The force dissipates quickly beyond the electrode. The time evolution of the force components due to charge separation is plotted in Fig. 4(b) for the positive half of the cycle at a point 1 mm downstream of the exposed electrode and 0.1 mm above the dielectric. The figure shows a steady rise and fall of the force following with the applied frequency. The negative half of the cycle is not shown as the magnitude of force is order of magnitude smaller in that segment. As the interelectrode gap d reduces the force increases, however the characteristic remains the same. The velocity field based on a quiescent flow initial condition shows streamwise component of the computed gas velocity in Fig. 5(a) and depicts a strong wall jet downstream of the rf electrode away from the dielectric surface. The highest momentum transfer between the gas and the charge particles occur slightly downstream of the peak force location. The local vertical line plots at six streamwise locations describe how the flow velocity increases responding to the increase in axial electric field [Fig. 5(b)] and experimental results show very similar feature.[1,2] The peak jet velocity is nearly 1.7 times the freestream velocity.

In conclusion, a 2D FE-based formulation of plasma-fluid interactions is given for modeling the dielectric barrier discharge for flow control purposes. The partially ionized plasma is modeled using the multicomponent fluid equation for helium gas. The computed results are similar to the experimental data showing the exposed electrode is situated upstream of the peak location of the electric field and thus the velocity. The 2D predictions mimic the self-limiting discharge mechanism due to the charge accumulation on the insulator surface and the lowest electron current just beyond the peak applied voltage. The results indicate that the surface charge on the dielectric is the key for unidirectional momentum transfer for asymmetric electrode configuration. A better selection of electrochemical data along with computation of electron temperature gradient is necessary for accuracy of the solution. More investigation is needed to ascertain the optimum electrical parameters and applied voltage shape (e.g., saw tooth, square wave, etc). In the near future, the model should be extended to air with negative ions and additional mechanisms in the source terms.

The author gratefully acknowledges many helpful discussions with Dr. Datta Gaitonde and Dr. Natalia Sternberg. This work was partially supported by the AFOSR Grant No. FA9550-05-1-0074 under tasks monitored by Dr. John Schmisseur, the Air Force Research Laboratory Contract No. F33615-98-D3210, the Summer Faculty sponsorship of VAAC during the summer of 2004, and the NRC/AFOSR research fellowship during the summer of 2003.

[1] J. R. Roth, Phys. Plasmas **10**, 2117 (2003).
[2] C. L. Enloe, T. E. McLaughlin, and R. D. VanDyken, AIAA J. **42**, 595 (2004).
[3] S. Roy and D. Gaitonde, J. Appl. Phys. **96**, 2476 (2004).
[4] K. Akhtar, J. E. Scharer, S. M. Tysk, and E. Kho, Rev. Sci. Instrum. **74**, 996 (2003).
[5] L. Ward, J. Appl. Phys. **33**, 2789 (1962).
[6] S. Roy, B. P. Pandey, J. Poggie, and D. Gaitonde, Phys. Plasmas **10**, 2578 (2003).
[7] S. Roy and B. P. Pandey, J. Propul. Power **19**, 964 (2003).
[8] S. M. Cooper, B. A. Cruden, M. Meyyappan, R. Raju, and S. Roy, Nano Lett. **4**, 377 (2004).
[9] D. Balagangadhar and S. Roy, Comput. Methods Appl. Mech. Eng. **190**, 5465 (2001).
[10] M. Riser, Comput. Methods Appl. Mech. Eng. **2**, 65 (1972).
[11] A. Bogaerts, E. Neyts, R. Gijbels, and J. van der Mullen, Spectrochim. Acta, Part B **57**, 609 (2002).
[12] F. Massines, A. Rabehi, P. Decomps, R. B. Gadri, P. Ségur, and C. Mayoux, J. Appl. Phys. **83**, 2950 (1998).